Crystal Structure of Human Heme Oxygenase-1 in a Complex with Biliverdin[†]

Latesh Lad,[‡] Jonathan Friedman,[‡] Huying Li,[‡] B. Bhaskar,[‡] Paul R. Ortiz de Montellano,[§] and Thomas L. Poulos*,[‡,||,⊥]

Departments of Molecular Biology and Biochemistry, Physiology and Biophysics, and Chemistry and the Program in Macromolecular Structure, University of California, Irvine, California 92697-3900, and Department of Pharmaceutical Chemistry, University of California, San Francisco, California 94143-2280

Received August 13, 2003; Revised Manuscript Received February 3, 2004

ABSTRACT: Heme oxygenase oxidatively cleaves heme to biliverdin, leading to the release of iron and CO through a process in which the heme participates both as a cofactor and as a substrate. Here we report the crystal structure of the product, iron-free biliverdin, in a complex with human HO-1 at 2.19 Å. Structural comparisons of the human biliverdin−HO-1 structure with its heme complex and the recently published rat HO-1 structure in a complex with the biliverdin−iron chelate [Sugishima, M., Sakamoto, H., Higashimoto, Y., Noguchi, M., and Fukuyama, K. (2003) *J. Biol. Chem. 278*, 32352−32358] show two major differences. First, in the absence of an Fe−His bond and solvent structure in the active site, the distal and proximal helices relax and adopt an "open" conformation which most likely encourages biliverdin release. Second, iron-free biliverdin occupies a different position and orientation relative to heme and the biliverdin−iron complex. Biliverdin adopts a more linear conformation and moves from the heme site to an internal cavity. These structural results provide insight into the rate-limiting step in HO-1 catalysis, which is product, biliverdin, release.

Heme oxygenase (HO)[1] catalyzes the NADPH, O_2, and cytochrome P450 reductase dependent oxygenation of heme to iron, biliverdin, and carbon monoxide (CO) (*1*) (Figure 1). The enzyme, which uses heme as both the prosthetic group and substrate, regiospecifically oxidizes the heme at the α-*meso* position. Biliverdin is reduced by biliverdin reductase to bilirubin, which is then excreted as the glucuronic acid conjugate (*2*). The excretion of bilirubin is frequently impaired in newborn children as well as in individuals with genetic glucuronyltransferase deficiencies (*3*). High concentrations of unconjugated bilirubin are neurotoxic, and the prevention of its accumulation through phototherapy or inhibition of heme oxygenase is of clinical importance (*3*, *4*). Although generally viewed as toxic, bilirubin and biliverdin can serve as potent antioxidants (*5*) by inhibiting superoxide production by neutrophils (*6*), quenching singlet molecular oxygen (*7*), and preventing lipid peroxidation (*8*). More recently, biliverdin and bilirubin have been implicated as effective modulators of cell signaling pathways, which includes activation of the aryl hydrocarbon receptor (*9*, *10*). The second product of the HO reaction,

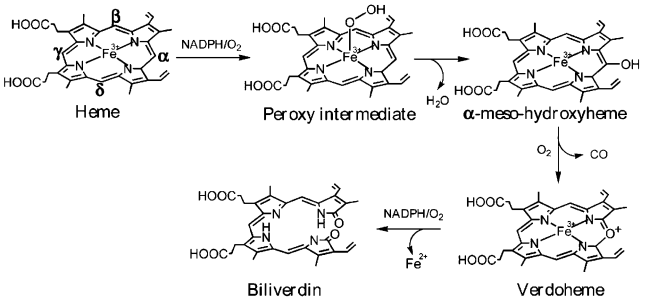

FIGURE 1: Overall reaction catalyzed by heme oxygenase that results in the oxidation of heme and release of the α-*meso* carbon atom as CO.

CO, affects the regulation of vessel tone (*10*, *12*) and blood pressure (*11*), whereas, on a more speculative note, CO has been suggested to serve as a signaling molecule through the guanylate cyclase system in a manner akin to nitric oxide (*12*, *15*). Lastly, the iron released by HO is normally recycled and represents the major source of this metal in heme homeostasis. However, increased iron release owing to elevated HO activity can also trigger enhanced lipid and protein peroxidation (*13*, *17*).

Mammals contain two HO isoforms denoted as HO-1 and HO-2 that exhibit essentially identical activity (*14*, *19*). Inducible HO-1 is involved primarily in heme catabolism in the liver and spleen, while the constitutive HO-2 is found in the brain and testes where it is proposed to function as a generator of CO (*3*, *15*). Both isoforms contain C-terminal hydrophobic sequences that provide anchors to the microsomal membrane. However, the expression of soluble, truncated forms of HO that lack the membrane binding domain while retaining activity (*16*) greatly facilitated detailed mechanistic studies of these enzymes. Most notable were the crystalliza-

[†] This work was supported by NIH Grants GM33688 (to T.L.P.) and DK30297 (to P.R.O.M.).

* To whom correspondence should be addressed: e-mail, poulos@uci.edu; tel, (949) 824-7020; fax, (949) 824-3280.

[‡] Department of Molecular Biology and Biochemistry and the Program in Macromolecular Structure, University of California, Irvine.

[§] Department of Pharmaceutical Chemistry, University of California, San Francisco.

[||] Department of Physiology and Biophysics, University of California, Irvine.

[⊥] Department of Chemistry, University of California, Irvine.

[1] Abbreviations: HO, heme oxygenase; HO-1, mammalian HO isozyme 1; CO, carbon monoxide; Fe, iron; BV, biliverdin; heme, iron protoporphyrin IX.

10.1021/bi035451l CCC: $27.50
Published on Web 03/06/2004

tion and structure determination of human and rat HO-1 enzymes complexed with heme (*17*), which provided significant insights into both the mechanism and regiospecificity of the HO reaction. The basic HO-1 catalyzed oxidation of heme involves rapid hydroxylation at the α-*meso* carbon of the heme, oxygen-dependent fragmentation of α-*meso*-hydroxyheme to verdoheme, and oxidative cleavage of verdoheme to biliverdin (*18*). The first electron provided by the P450 reductase reduces the ferric heme iron to the ferrous state, and a molecule of oxygen binds to form a metastable O_2-bound complex which is reduced by a second electron to generate ferric hydroperoxy HO [Fe(III)-OOH] (*19*). According to detailed spectroscopic studies (*20*), the next step is electrophilic addition of the reactive Fe(III)-OOH species to the heme α-*meso* carbon. This is in contrast to peroxidases and cytochrome P450 that proceed through a high-valent ferryl [Fe(IV)-O] active intermediate (*21*) as the reactive hydroxylating species rather than a peroxo ligand capable of attacking the α-*meso* bridge of the heme (Figure 1). The exact stoichiometric requirements involved in the formation of ferric verdoheme from α-*meso*-hydroxyheme have been controversial (*22*). Although there is general agreement that this process is oxygen-dependent, the suggestion that additional reducing equivalents are also required (*23*) has been questioned (*24*). The conversion of verdoheme to biliverdin is the least well-characterized step of the overall reaction, although a mechanism has been proposed (*25*).

Since the initial publication of the human and rat heme−HO-1 structures a wealth of structural (*26*−*31*) and mutagenic (*32*, *33*) information has emerged that has greatly improved our overall understanding of these enzymes, especially the regioselective hydroxylation reaction. To briefly summarize, flexibility in the heme pocket, especially the distal helix, helps to trap important water molecules in the active site that form a conserved H-bonded network with key amino side chains such as Asp 140 in HO-1. The purpose of this network is to deliver a proton to the iron-linked dioxygen required for catalysis. This H-bonded network together with steric factors orient dioxygen or peroxide toward the α-*meso* heme carbon for regioselective electrophilic attack by the distal peroxide OH group. Significant advances also have been made in understanding the conversion of hydroxyheme to verdoheme (*34*). However, the mechanism whereby biliverdin is produced still remains relatively unclear. The recent publication of the crystal structure of rat HO-1 in a complex with iron(III) biliverdin bound in the active site has shed some light on this matter (*29*). Here we report the crystal structure of human HO-1 in a complex with iron-free biliverdin at 2.19 Å resolution. Comparison of the iron-free and iron-bound biliverdin−HO-1 structures provides a more complete picture of the final step in the heme degradation pathway.

MATERIALS AND METHODS

Bacterial Expression and Protein Purification. Bacterial fermentation and purification of HO-1 was carried out according to published procedures (*35*). Enzyme purity was assessed using SDS−PAGE, and all preparations were judged to be homogeneous by the observation of a single band on a Coomassie Blue-stained reducing SDS−PAGE gel.

Crystallization. A complex of biliverdin with human HO-1 was formed using three different methods. The first biliverdin−HO-1 complex, termed BV1, was prepared by adding biliverdin (predissolved in 0.1 M NaOH) to pure apo-HO-1 protein to give a final 4:1 biliverdin to apoprotein ratio. The resulting complex was dialyzed against 10 mM potassium phosphate, pH 7.4, and free biliverdin was removed by passing the complex down a Sephadex G-25 column preequilibrated with 10 mM potassium phosphate, pH 7.4. The second complex, BV2, was prepared using a coupled oxidation system by adding a 200-fold excess of ascorbate to the Fe^{3+}−heme HO-1 complex at pH 7.4. Conversion of heme to biliverdin was complete in less than 1 h at room temperature and was confirmed by a color change from red to green and by a distinct UV−visible spectrum with broad peaks at 387 and 680 nm. Free ascorbate was removed by passing the complex mixture down a Sephadex G-25 column preequilibrated with 10 mM potassium phosphate, pH 7.4. The final biliverdin−HO-1 complex, BV3, was obtained directly from the expressed human HO-1 protein. *Escherichia coli* is able to support the HO-1 reaction and as a result recombinantly expressed HO-1 has biliverdin bound. Cells were lysed and resuspended as previously described (*35*). However, rather than removing biliverdin, the protein was first applied to a Bio-Gel HTP column preequilibrated with 10 mM potassium phosphate, pH 7.7. The column was then washed with the same buffer until no biliverdin could be detected in the eluent. The biliverdin−HO-1 complex was finally eluted with 90 mM potassium phosphate, pH 7.4. Protein purity was checked by SDS−PAGE, and pure fractions were pooled, then dialyzed against 10 mM potassium phosphate, pH 7.4, and concentrated to 1 mL. The concentrated protein was further purified by S-100 gel filtration chromatography in 10 mM potassium phosphate, pH 7.4. Finally, to ensure appropriate levels of biliverdin in BV3, BV3 was reconstituted with biliverdin, with the excess being removed by passing the complex down a Sephadex G-25 column preequilibrated with 10 mM potassium phosphate, pH 7.4.

The biliverdin−HO-1 complexes were crystallized in a manner similar to that described by Schuller et al. (*35*). Briefly, the sitting-drop vapor diffusion method was used with a well solution of 2.08 M ammonium sulfate, 100 mM HEPES (pH 7.5), and 0.9% 1,6-hexanediol. Drops consisted of protein stock (5 μL) at 45 mg mL^{-1} in 20 mM potassium phosphate (pH 7.4), mixed with well solution (5 μL) on siliconized coverslips. Under these conditions we observed sporadic crystal growth of tightly stacked plates. One round of touch seeding and, if necessary, one round of macroseeding after a 24 h incubation period produced single plates. For cryogenic data collection biliverdin−HO-1 complex crystals were transferred stepwise in 5% increments to artificial precipitant solution of D-(+)-trehalose concentration up to 35% (v/v) D-(+)-trehalose incorporated with 1 mM biliverdin. Biliverdin−HO-1 crystals belong to the monoclinic space group $P2_1$ (cell dimensions listed in Table 1).

Data Collection. In-house data were collected using an R-AXIS IV imaging plate detector equipped with a rotating copper anode X-ray generator with Osmic optics (Rigaku). Crystals were maintained at −160 °C in a steam of nitrogen (Crystal Logic, Los Angeles, CA). High-resolution data collection was performed at ALS beamline 5.0.2 with a

Table 1: Data Collection and Refinement Statistics[a]

	holo	apo	BV1	BV2	BV3
PDB code	1QQ8	1N16			1S8C
crystal data					
radiation source	synchrotron	in house	in house	synchrotron	synchrotron
space group	$P2_1$	$P2_1$	$P2_1$	$P2_1$	$P2_1$
cell parameters					
a (Å)	61.44	76.21	77.01	77.97	77.41
b (Å)	54.53	55.51	56.05	56.70	56.46
c (Å)	70.97	108.00	109.45	109.76	109.75
β (deg)	99.05	98.88	99.99	101.18	100.39
data collection					
detector distance (nm)	130	140	140	150	150
molecules per asymmetric unit	2	4	4	4	4
resolution (Å)	1.50	2.10	2.54	2.31	2.19
mosaicity (deg)	0.46	0.70	1.11	0.98	0.89
total observations	273199	519735	118576	133429	197925
unique reflections	74186	49421	30135	39235	55836
completeness (%)	99.7	94.0	93.5	95.0	96.7
mean I/σ[b]	11.4 (2.12)	20.6 (2.02)	24.2 (1.97)	11.0 (4.6)	17.3 (3.3)
R_{sym} (%)[b]	5.1 (48.4)	6.8 (55.9)	6.2 (61.4)	5.9 (43.0)	5.6 (50.9)
refinement statistics					
R_{cryst}[c]	0.159	0.217	0.242	0.221	0.233
R_{free}	0.193	0.262	0.298	0.268	0.264
rms[d] bond lengths (Å)	0.006	0.006	0.008	0.006	0.006
rms[d] angles (deg)	1.1	1.1	1.3	1.2	1.2
water molecules	494	450	82	303	359
Ramachandran angles					
most favored (%)	93.8	92.3	91.8	91.8	92.4
additionally allowed (%)	6.2	7.5	8.0	7.8	7.3
generously allowed (%)	0.0	0.3	0.2	0.4	0.3

[a] Data collection statistics for the heme−HO-1 and apo-HO-1 were previously reported (*31*) and are reproduced here for convenience. [b] Values in parentheses are for the outermost shell. [c] $R_{cryst} = \sum(|F_o| - |F_c|)/\sum|F_o|$. The R_{free} is the R_{cryst} calculated on the 5% reflections excluded for refinement. [d] rms bond and rms angle represent the root-mean-squared deviation between the observed and ideal values.

charge-coupled device (CCD). Optimization of data collection was guided by the STRATEGY function of MOSFLM (*36*). All data were reduced using HKL 2000 (*37*), and rejections were performed with ENDHKL (Louis Sanchez, California Institute of Technology) in conjunction with SCALEPACK. For all data collection, a 180° scan using 1° frames was collected.

Model Building and Refinement. The crystal structure of BV2 was determined by the method of molecular replacement using MOLREP (*38*). A monomer of the human heme−HO-1 crystal structure (PDB number 1qq8) (*39*), with the heme and waters removed, was used as the probe, with searches being carried out at 4 Å in space group $P2_1$. The best cross-rotation and translation function solution was rigid body refined and fixed in place, followed by a search for the remaining molecules in the asymmetric unit. A total of four solutions were found, corresponding to the expected four monomers per asymmetric unit. The final R factor was 42.9% with a correlation coefficient of 50.4%. The structure was further refined in CNS (*40*). Protein atoms were initially refined by simulated annealing, followed by a few cycles of conjugate gradient minimization and water picking. Finally, temperature factors were refined. During refinement no restraints for noncrystallographic symmetry were applied.

Crystal structures for BV1 and BV3 were determined in CNS with the apo human heme−HO-1 crystal structure (PDB number 1n16) (*27*), with all ligands and waters removed, used as the starting model. With all structures the maximum likelihood target function was used for the refinement with all of the observed reflections included in the calculations. The program O (*41*) was used for further adjustment and modeling of protein atoms, biliverdin, and water molecules. Backbone geometry was checked in PROCHECK (*42*), and none of the residues were in the disallowed region. In the case for BV3, the binding of biliverdin was confirmed toward the end of the refinement by calculating omit maps with a simulated annealing protocol at a starting temperature of 1000 K. The composite omit electron density map for the biliverdin ligand in molecule A of BV3 is shown in Figure 2A. Data collection and refinement statistics are summarized in Table 1.

RESULTS

Overall Structure and Crystallization. Formation and crystallization of a biliverdin−heme oxygenase complex were successfully achieved in three ways (see Materials and Methods): cocrystallization of biliverdin with apo human HO-1 (BV1), ascorbate-driven reaction to a solution of human heme−HO-1 prior to crystallization (BV2), and purification and crystallization of biliverdin−HO-1 accumulated during human HO-1 expression (BV3). However, from the crystallized complexes we observe interpretable electron density for biliverdin only in complex BV3 (Figure 2A) even though the remaining complexes have biliverdin present in a 1:1 ratio with protein (Figure 2B). It should be noted that the density observed for biliverdin in BV3 also appears in the same location in the protein molecules of BV1 and BV2 but is not sufficiently clear to enable an unambiguous positioning of biliverdin. For this reason the remaining part of this paper will describe the crystal structure of BV3. The BV3 structure has been refined to an R factor of 0.23 and a free R factor of 0.26 at 2.19 Å resolution. The final structure contains four molecules in the asymmetric unit (labeled A−D) with a total of 6977 protein atoms and 359

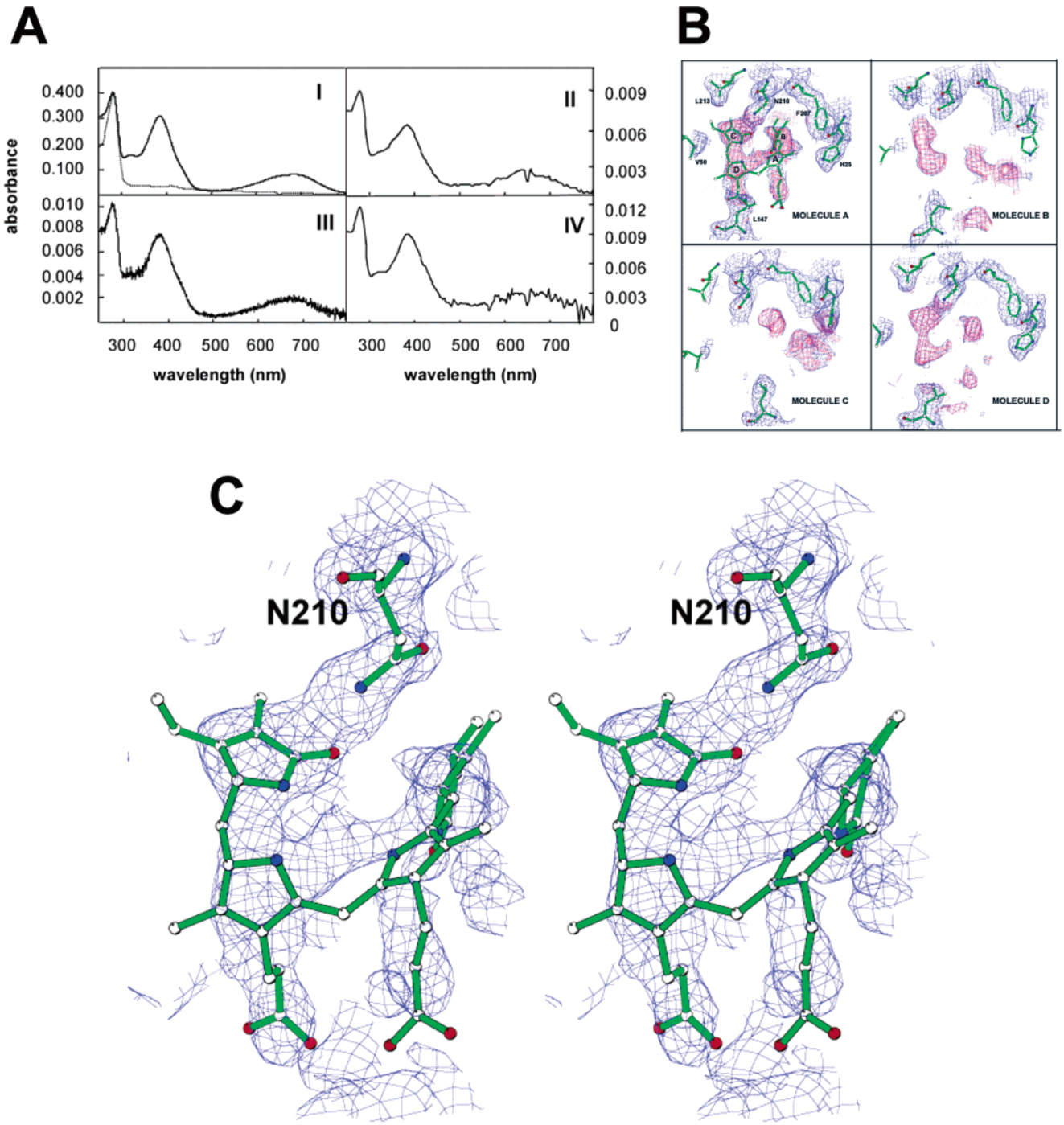

FIGURE 2: (A) UV−visible spectra of the various crystallization complexes of biliverdin−HO-1 after data collection (20 mM potassium phosphate buffer, pH 7.5, 20 °C): (I) for comparison, solution spectra of apo-HO-1 (dotted line) and 1:1 ratio of biliverdin in a complex with human HO-1 (solid line); (II) dissolved single crystal of BV1; (III) dissolved single crystal of BV2; (IV) dissolved single crystal of BV3. (B) Monoviews of the composite omit maps for all four molecules in the asymmetric unit. $F_o - F_c$ maps (red) are contoured at 3.0σ while $2F_o - F_c$ (blue) are contoured at 1.0σ. (C) Stereo diagram of the $2F_o - F_c$ composite omit electron density contoured at 1σ around biliverdin in biliverdin−HO-1 of molecule A. All of the figures in this paper were prepared with MOLSCRIPT (*50*) and Raster3D (*51*).

water atoms. In all four molecules the first 9 and last 10 residues of the 233-residue protein are not ordered. While electron density for biliverdin is present in all four molecules, molecule A has the clearest biliverdin electron density, and as a result, only molecule A of this structure will be compared and discussed. We attribute this difference primarily to crystal packing. The active site opening in molecule A is more closely surrounded by other molecules in the asymmetric unit which very likely helped to trap biliverdin in the active site. Despite these differences, the overall average root mean square deviation of backbone atoms between the four molecules (A−B, A−C, and A−D) is very low, 0.31 Å.

Distal and Proximal Helices. An important feature of the human HO-1 structure is the distal helical region that covers part of the distal heme surface as well as forming an integral part of the oxygen-binding pocket (*39*). In the human heme−HO-1 structure the two molecules in the asymmetric unit are referred to as being either open or closed, based upon the position of the distal helix. In the closed conformation,

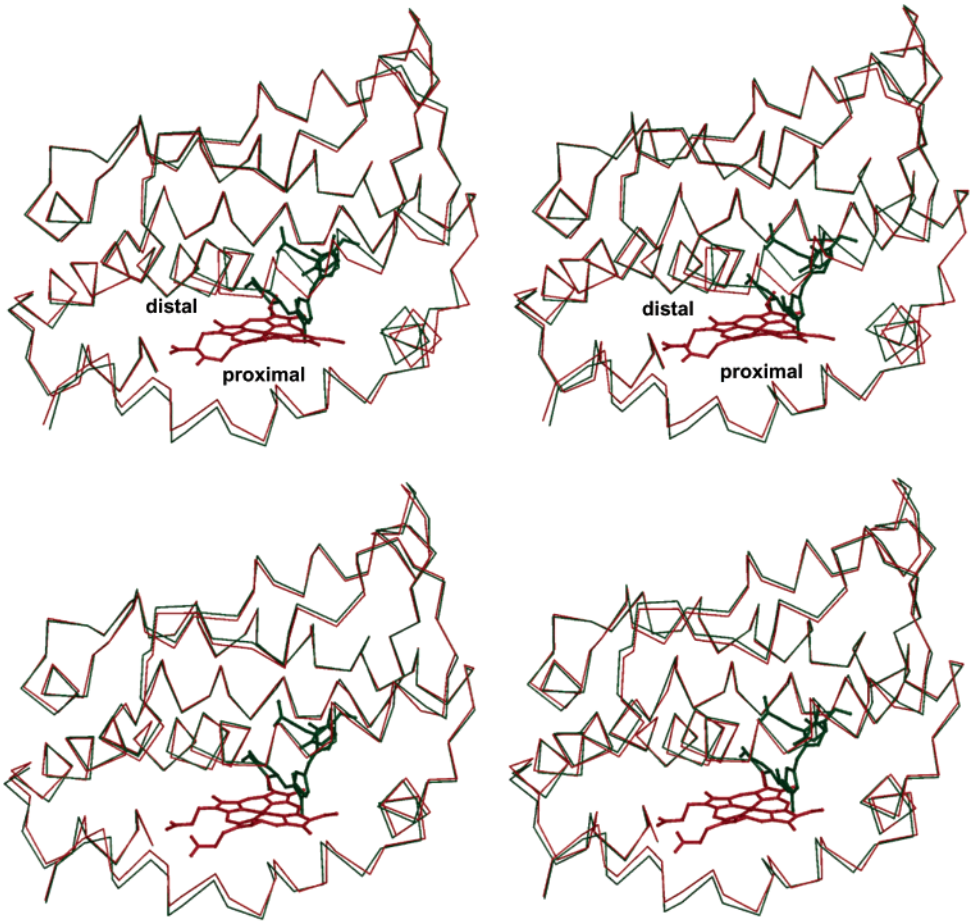

FIGURE 3: Comparisons of the human heme and biliverdin−HO-1 structures. Stereo diagram least-squares superimposition of biliverdin−HO-1 with the closed conformation of heme−HO-1 (top) and open conformation of heme−HO-1 (bottom).

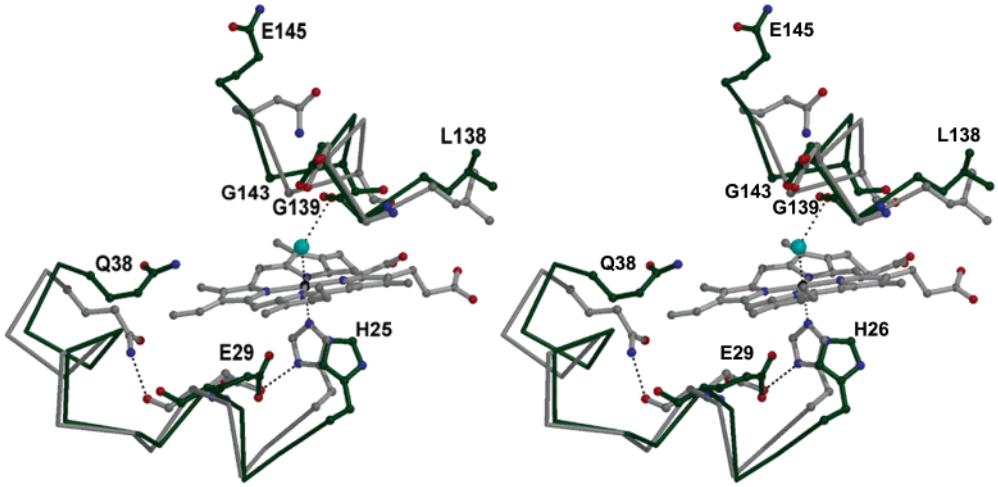

FIGURE 4: Stereo diagram comparing the distal and proximal heme region between the closed conformation of the heme−HO-1 structure (gray) and biliverdin−HO-1 (green). Hydrogen bonds are represented as dashed lines.

the distal helix is closer to the heme, thus forming a slightly tighter active site pocket. Figure 3 (top) shows a comparison of closed and open molecules of human heme−HO-1 with biliverdin−HO-1. The overall structure of human biliverdin−HO-1 is very similar to the heme−HO-1 structure (root mean square deviation for Cα atoms being 0.52 Å for the closed molecule and 0.39 Å for the open molecule). There is a large deviation in the proximal helix (residues 20−30), but only when compared to the closed heme−HO-1 molecule do we observe large deviations in the distal helix and following loop (residues 139−157). In the biliverdin−HO-1 structure the distal and proximal helices have loosened to adopt an open conformation similar to apo-HO-1 (*27*). Figure 4 provides a close-up view of the distal and proximal helices. The backbone atoms of Gly 143 and Gly 139, which in the closed molecule of the heme−HO-1 structure directly contact the heme, have shifted away in the biliverdin−HO-1 structure although the kink in the distal helix is maintained. In the closed molecule of heme−HO-1 Ser 142 helps to maintain the distal helix distortion primarily through H-bonding

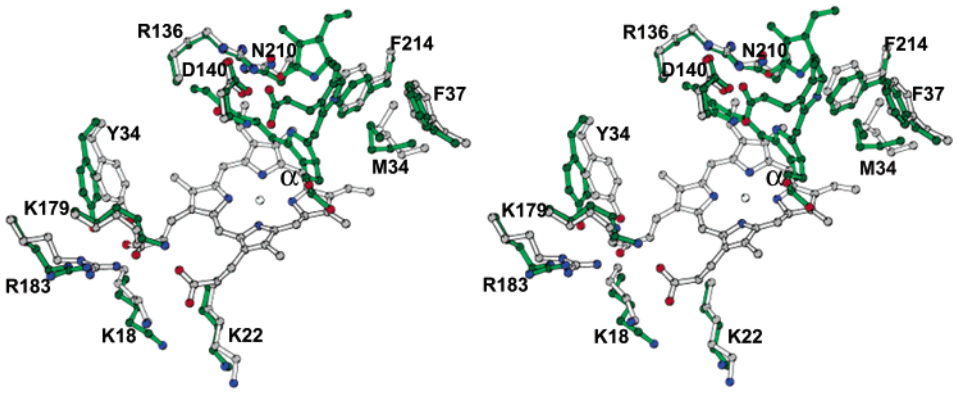

FIGURE 5: Stereo diagram of the heme and biliverdin binding locations in human HO-1. Comparison of the heme pocket region between the closed conformation of heme−HO-1 (gray) and the biliverdin−HO-1 structure (green).

interactions with the peptide backbone of Gly 143, Leu 138, and Glu 145. In biliverdin−HO-1 the interaction between Ser 142 and Glu 145 is lost, causing the side chain of Glu 145 to rotate and point in the opposite direction. The original interaction between Ser 142 and Leu 138 is maintained, but the nonbonded contact with the C-δ1 atom of Leu 138 is broken, causing the side chain of this residue to move away from the heme site.

Despite these changes in the distal pocket, key catalytic groups remain unchanged. The most important is Asp 140, which is essential in the activation of the HO peroxy intermediate by a mechanism involving the hydrogen-bonding network of the bridging waters and the Asp 140 carboxylate side chain (*43*). Although Asp 140 remains fixed in place, rigid and catalytically important solvent structure present in the heme−HO-1 active site is lost in biliverdin−HO-1. In particular are the key waters present near the Asp 140 side chain that play a crucial role in the activation of oxygen (*31*).

On the proximal side the histidine ligand (His 25) moves away from the heme pocket. The hydrogen bond between Glu 29 and His 25 in heme−HO-1 is lost in the biliverdin−HO-1 structure. In addition, the side chain of Gln 38, located near pyrrole A in the vicinity of the δ-*meso* carbon, points down toward the proximal helix, enabling it to be H-bonded with the carbonyl oxygen of Glu 29 in the closed molecule of heme−HO-1. In the biliverdin−HO-1 structure the same residue has its side chain pointing up, and the bonding interaction with Glu 29 is lost (Figure 4).

Heme Binding Site. In the heme−HO-1 structure the heme is only partially buried in the protein. Three of the four *meso* edges are buried in the protein, while one, the δ-*meso* edge, is exposed along with the heme propionates (Figures 5). The α-*meso* edge of the heme, which is selectively targeted for hydroxylation in the HO reaction, faces a wall of hydrophobic residues in the protein interior consisting of Phe 214, Met 34, and Phe 37 (Figures 5). In biliverdin−HO-1 these residues remain relatively unchanged. On the opposite side of the heme a number of ionic/H-bonding interactions between the heme propionates and nearby side chains are important for orientating the heme in the active site. Basic residues Arg 183, Lys 18, and Lys 22 surround the propionates, thus holding the heme in place in the heme−HO-1 structure. In the biliverdin−HO-1 structure several of these residues have changed. Residues such as Arg 183, Lys 179, Lys 18, and Lys 22 have either turned or moved away from their positions in the heme−HO-1 structure (Figure 5). Also in contact with the heme propionates in the heme−HO-1 structure is Tyr 134. In the biliverdin−HO-1 structure the aromatic ring of Tyr 134 clearly leans away from the heme propionates, and its movement results in a reorientation of Thr 135.

Biliverdin Binding Site. The movement of the distal and proximal helices, absence of solvent structure in the active site, and loss of direct interactions with the heme propionates and heme iron increase the overall size of the HO-1 active site, thus allowing biliverdin to adopt a totally different binding location. Although the spectroscopic data clearly indicate that a full equivalent of biliverdin is bound, the electron density is not sufficiently clear to enable an unambiguous positioning of the biliverdin. This very likely is the result of high mobility and, possibly, multiple binding modes. Even so, the positioning of one of the heme propionates and the pyrrole ring containing one of the lactam oxygen atoms is clear because the lactam oxygen is close enough to Asn 210 to accept an H-bond (Figure 2C). While the detailed interactions between biliverdin and protein cannot unambiguously be assigned, it is clear that biliverdin adopts a twisted conformation and is more buried than the heme. In the heme−HO-1 structure the heme is only partially buried in the active site with the δ-*meso* heme edge and propionates exposed at the molecular surface. The total solvent-accessible surface area of the heme is 145 Å^2. In biliverdin−HO-1 the biliverdin adopts a nonplanar curled conformation and moves further into the active site to occupy a large internal cavity that in the heme−HO-1 complex sits above the α-*meso* heme carbon, and the solvent-accessible surface area decreases to 45 Å^2 (Figures 2C and 5). Without the iron to coordinate the biliverdin and His ligand, the heme pocket cannot provide sufficiently favorable interactions to hold biliverdin within the heme site.

Comparison to Other Biliverdin (Iron-Free) Structures. The structure of biliverdin in biliverdin−HO-1 is somewhat atypical to that previously reported for protein structures cocrystallized with either biliverdin or ferric biliverdin or the lone structure of biliverdin itself (*44*). In such proteins biliverdin adopts an almost all-*Z*-all-*syn* type conformation, similar to heme itself, with the exception being that the rings containing the lactam oxygens must twist in order to avoid collision between the lactam oxygen atoms. In the biliverdin−HO-1 structure, biliverdin does not adopt a planar conformation with each of the pyrrole rings twisted in and

out of the plane with respect to one another. In the biliverdin−HO-1 complex the twist resembles a left-handed helix which places the lactam oxygen atoms about 5 Å apart compared to 3.3 Å for rat biliverdin(Fe)−HO-1 (*29*), 3.0 Å in the apomyoglobin−biliverdin complex (*44*), 2.8 Å in the biliverdin IXβ reductase (*45*), and 3.4 Å in the crystal structure of biliverdin dimethyl ester (*46*). Biliverdin is a flexible molecule which should be able to adopt a number of near isoenergetic conformations ranging from heme-like to linear. That the biliverdin−HO-1 complex exhibits the more linear conformation is very likely due to the lack of extensive protein−heme nonbonded contacts than in proteins such as myoglobin which are designed to firmly hold the heme in place. This also helps to understand why the electron density for biliverdin is weak even though the spectroscopy clearly shows that a full equivalent of biliverdin is bound to HO-1.

DISCUSSION

Recent crystallographic results (*31*) combined with mutagenic studies have substantially advanced our overall understanding of HO catalysis, especially the steps leading to the regiospecific hydroxylation of heme. Although crystallographic information is not yet available for the HO catalytic intermediates α-*meso*-hydroxyheme and verdoheme, detailed spectroscopic and mechanistic studies have provided valuable information detailing the structural and functional requirements of these intermediates during catalysis (*47*). The least well-known step during HO catalysis is the conversion of verdoheme to biliverdin. This step is known to require oxygen and reducing equivalents (*47*), but very little is known about the mechanism whereby biliverdin is produced from verdoheme and finally released from the enzyme. Coupled with the recent work on the structure of the iron(III) biliverdin−HO-1 complex (*29*), our present work provides a more detailed picture on the release of biliverdin during HO catalysis.

Biliverdin−HO-1 vs Heme−HO-1. The most unexpected finding is the conformation and location of biliverdin compared to other biliverdin−protein complexes and movement of biliverdin into an internal cavity. For example, in the biliverdin−myoglobin complex (*44*) the biliverdin adopts a planar heme-like conformation. In the rat iron(III) biliverdin complex the iron(III) biliverdin also adopts a planar heme-like conformation and binds in the same pocket as the heme and retains the His ligand−Fe iron interaction although at a longer distance of 2.44 Å. Clearly, the protein−biliverdin interactions in myoglobin are sufficiently strong to maintain biliverdin in the planar configuration while this is not the case with HO-1. The heme in myoglobin is substantially more buried than the heme in heme−HO-1, and hence, there are fewer nonbonded contacts in HO-1 to help hold the biliverdin in a planar conformation. In addition, myoglobin lacks the large internal cavity found in HO-1 that provides the additional room for biliverdin to adopt the more linear conformation. As the rat iron(III) biliverdin−HO-1 structure and our presents studies show, the iron must be present in order for biliverdin to maintain a planar conformation.

Owing to the lack of strong interactions to maintain a planar conformation, the biliverdin adopts an energetically more favorable extended but curled conformation. This requires many changes in the active site, which includes the movement of key basic side chains that are used to interact with the propionates and properly orient the heme and a widening of the active site from 43.6 A^3 in heme−HO-1 to 61.2 A^3 in biliverdin−HO-1, which allows more room for biliverdin to move out of the heme site to the internal pocket. The key feature in the location and partial burial of biliverdin is the introduction of two carbonyl groups, the biliverdin lactam oxygens. The heme in heme−HO-1 sits just below a tier of polar residues consisting of Arg 136, Asp 140, and Asn 210, which are also involved in a network of polar interactions with a second tier of residues that includes Tyr 58 and Tyr 114. We postulate that when the heme is cleaved, producing biliverdin, the lactam oxygens of biliverdin are stabilized by a cluster of internal polar residues, Asp 140, Arg 136, and Asn 210, which partly accounts for the observed curled conformation and partial burial. The fairly high *B* factors and poor electron density for parts of the biliverdin clearly indicate that the biliverdin does not form many specific interactions and, hence, is not tightly bound. In summary, it appears that the observed binding site and conformation of biliverdin are energetic defaults. Biliverdin probably prefers a linear as opposed to the flat conformation, but since HO-1 cannot provide enough interactions to hold biliverdin in the planar conformation, biliverdin must seek out an alternate binding mode that requires the product to adopt the more favorable partial linear conformation. This further requires burial and the formation of fairly weak protein−biliverdin interactions.

Biliverdin−HO-1 vs Iron(III) Biliverdin−HO-1: Catalytic Implications for Product Release. Once iron(III) biliverdin is formed, the next step in the HO catalytic cycle is reduction and release of the iron (*48*) from iron(II) biliverdin. As already noted, the rat iron(III) biliverdin−HO-1 shows that iron(III) biliverdin forms many of the same interactions as heme and retains a near planar conformation. Our present work shows that once the iron is reduced and released, the biliverdin adopts a totally different conformation and binding mode. The main question is whether the binding mode we observe is physiologically relevant. Detailed kinetic studies show that (*48*) in the presence of biliverdin reductase the rate-limiting step is the conversion of ferrous verdoheme to iron(III) biliverdin. However, in the absence of biliverdin reductase dissociation of biliverdin is the rate-limiting step. The dissociation of biliverdin from the internal pocket observed in the present study is undoubtedly a slow process and is the reason dissociation of biliverdin is rate-limiting. When biliverdin reductase is present, it very likely forms a complex with HO-1 near the active site which facilitates biliverdin release. Indeed, recent binding experiments between biliverdin reductase and human HO-1 have shown that human HO-1 and biliverdin reductase do form a tight protein−protein complex (K_d = 0.2−0.5 μM) and that biliverdin reductase binds to the exposed molecular surface of the heme binding pocket where residues Lys 18, Lys 22, Lys 179, Arg 183, and Arg 185 of human HO-1 are particularly important for efficient binding between the two proteins (*49*). This would indicate that in the presence of biliverdin reductase the biliverdin may never adopt the linear conformation and move into the internal cavity but instead is rapidly removed by biliverdin reductase. Given this

scenario, the binding mode we observe is not physiologically relevant.

The true scenario is very likely more complex. P450 reductase also is thought to bind to the same surface of HO-1 as biliverdin reductase (*39*). Therefore, P450 reductase must first bind, reduce the iron, and dissociate, and then biliverdin reductase must bind. It seems unlikely that multiple second-order binding/dissociation events between proteins occur faster than biliverdin can adopt the linear conformation and move into the internal cavity especially since this is a first-order unimolecular process. Thus, biliverdin reductase more likely binds to HO-1 after biliverdin has moved into the internal cavity. We therefore suggest that the binding mode we observe in HO-1 for biliverdin provides a way to temporarily but loosely hold biliverdin until biliverdin reductase can bind and remove biliverdin for further processing. On a more teleological note, this view provides a reason HO-1 has such a large internal cavity.

ACKNOWLEDGMENT

We thank Jayshali Lad for technical assistance during data collection and protein purification. We are extremely grateful to Prof. Fukuyama for giving us the PDB coordinates of rat HO-1 in a complex with biliverdin−iron chelate before official release.

REFERENCES

1. Tenhunen, R., Marver, H. S., and Schmid, R. (1969) Microsomal heme oxygenase. Characterization of the enzyme, *J. Biol. Chem. 244*, 6388−6394.
2. Schmid, R., and McDonagh, A. F. (1979) *The Porphyrins* (Dolphin, D., Ed.) Vol. VI, pp 257−292, Academic Press, New York.
3. Maines, M. D. (1992) *Heme Oxygenase: Clinical Applications and Functions*, pp 203−266, CRC Press, Boca Raton, FL.
4. Drummond, G. S., and Kappas, A. (1981) Prevention of neonatal hyperbilirubinemia by tin protoporphyrin IX, a potent competitive inhibitor of heme oxidation, *Proc. Natl. Acad. Sci. U.S.A. 78*, 6466−6470.
5. Neuzil, J., and Stocker, R. (1994) Free and albumin-bound bilirubin are efficient co-antioxidants for a-tocopherol, inhibiting plasma and low-density lipoprotein lipid peroxidation, *J. Biol. Chem 269*, 16712−16719.
6. Kwak, J. Y., Takeshige, K., Cheung, B. S., and Minakami, S. (1991) Bilirubin inhibits the activation of superoxide-producing NADPH oxidase in a neutrophils cell free-system, *Biochim. Biophys. Acta 1076*, 369−373.
7. Di-Mascio, P., Devasagayam, T. P., Kaiser, S., and Sies, H. (1990) Carotenoids, tocopherols and thiols as biological singlet molecular oxygen quenchers, *Biochem. Soc. Trans. 18*, 1054−1056.
8. Stocker, R., and Peterhans, E. (1989) Synergistic interaction between Vitamin E and the bile pigments bilirubin and biliverdin, *Biochim. Biophys. Acta 1002*, 238−244.
9. Phelan, D., Winter, G. M., Rogers, W. J., Lam, J. C., and Denison, M. S. (1998) Activation of the Ah receptor signal transduction pathway by bilirubin and biliverdin, *Arch. Biochem. Biophys. 357*, 155−163.
10. Wakabayashi, Y., Takamiya, R., Mizuki, A., Kyokane, T., Goda, N., Yamaguchi, T., Takeoka, S., Tsuchida, E., Suematsu, M., and Ishimura, Y. (1999) Carbon monoxide overproduced by heme oxygenase-1 causes a reduction of vascular resistance in perfused rat liver, *Am. J. Physiol 277*, 1088−1096.
11. Motterlini, R., Gonzales, A., Foresti, R., Clark, J. E., Green, C. J., and Winslow, R. M. (1998) Heme oxygenase-1-derived carbon monoxide contributes to the suppression of acute hypertensive responses in vivo, *Circ. Res. 83*, 568−577.
12. Maines, M. D. (1997) The heme oxygenase system: A regulator of second messenger gases, *Annu. Rev. Pharmacol. Toxicol. 37*, 517−554.
13. Mireles, L. C., Lum, M. A., and Dennery, P. A. (1999) Antioxidant and cytotoxic effects of bilirubin on neonatal erythrocytes, *Pediatr. Res. 45*, 355−362.
14. Shibahara, S., Müller, R., Taguchi, H., and Yoshida, T. (1985) Cloning and expression of cDNA for rat heme oxygenase, *Proc. Natl. Acad. Sci. U.S.A. 82*, 7865−7869.
15. Suematsu, M., and Ishimura, Y. (2000) The heme oxygenase-carbon monoxide system: a regulator of hepatobilary funation, *Hepatology 31*, 3−6.
16. Wilks, A., Black, S. M., Miller, W. L., and Ortiz de Montellano, P. R. (1995) Expression and characterization of truncated human heme oxygenase hHO-1 and a fusion protein of hHO-1 with human cytochrome P450 reductase, *Biochemistry 34*, 4421−4427.
17. Sugishima, M., Omata, Y., Kakuta, Y., Sakamoto, H., Noguchi, M., and Fukuyama, K. (2000) Crystal structure of rat heme oxygenase-1 in complex with heme, *FEBS Lett. 471*, 61−66.
18. Ortiz de Montellano, P. R. (2000) The mechanism of heme oxygenase, *Curr. Opin. Chem. Biol. 4*, 221−227.
19. Yoshida, T., Noguchi, M., and Kikuchi, G. (1980) Oxygenated form of heme−heme oxygenase complex and requirement for second electron to initiate heme degradation from the oxygenated complex, *J. Biol. Chem. 255*, 4418−4420.
20. Davydov, R. M., Yoshida, T., Ikeda-Saito, M., and Hoffman, B. M. (1999) Hydroperoxy-heme oxygenase generated by cryoreduction catalyzes the formation of α-*meso*-hydroxyheme as detected by EPR and ENDOR, *J. Am. Chem. Soc. 121*, 10656−10657.
21. Wilks, A., Torpey, J., and Ortiz de Montellano, P. R. (1994) Heme oxygenase HO-1. Evidence for electrophilic oxygen addition to the porphyrin ring in the formation of α-*meso*-hydroxyheme, *J. Biol. Chem. 269*, 29553−29556.
22. Sakamoto, H., Omata, Y., Palmer, G., and Noguchi, M. (1999) Ferric α-hydroxyheme bound to heme oxygenase can be converted to verdoheme by dioxygen in the absence of added reducing equivalents, *J. Biol. Chem. 274*, 18196−18200.
23. Migita, C. T., Fujii, H., Matera, K. M., Takahashi, S., Zhou, H., and Yoshida, T. (1999) Molecular oxygen oxidizes the porphyrin ring of the ferric α-hydroxyheme in heme oxygenase in the absence of reducing equivalents. *Biochim. Biophys. Acta 1432*, 203−213.
24. Liu, Y., Moënne-Loccoz, P., Loehr, T. M., and Ortiz de Montellano, P. R. (1997) Heme oxygenase-1, intermediates in verdoheme formation and the requirement for reduction equivalents, *J. Biol. Chem. 272*, 6909−6917.
25. Ortiz de Montellano, P. R. (1998) Heme oxygenase mechanism: evidence for an electrophilic ferric peroxide species, *Acc. Chem. Res. 31*, 543−549.
26. Sugishima, M., Sakamoto, H., Kakuta, Y., Omata, Y., Hayashi, S., Noguchi, M., and Fukuyama, K. (2002) Crystal structure of rat apo-heme oxygenase (HO-1): Mechanism of heme binding in HO-1 inferred from structural comparison of the apo and heme complex forms, *Biochemistry 41*, 7293−7300.
27. Lad, L., Schuller, D. J., Friedman, J., Shimizu, H., Li, H., Ortiz de Montellano, P. R., and Poulos, T. L. (2003) Comparison of the heme-free and -bound crystal structures of human heme oxygenase-1, *J. Biol. Chem. 278*, 7834−7843.
28. Sugishima, M., Sakamoto, H., Higashimoto, Y., Omata, Y., Hayashi, S., Noguchi, M., and Fukuyama, K. (2002) Crystal structure of rat heme oxygenase-1 in complex with heme bound to azide: implication for regiospecific hydroxylation of heme at the α-*meso* carbon, *J. Biol. Chem. 277*, 45086−45090.
29. Sugishima, M., Sakamoto, H., Higashimoto, Y., Noguchi, M., and Fukuyama, K. (2003) Crystal Structure of Rat Heme Oxygenase-1 in Complex with Biliverdin-Iron Chelate, *J. Biol. Chem. 278*, 32352−32358.
30. Friedman, J., Lad, L., Deshmukh, R., Li, H., Wilks, A., and Poulos, T. L. (2003) Crystal structures of the NO- and CO-bound heme oxygenase from *Neisseriae meningitidis*: Implications for oxygen activation, *J. Biol. Chem. 278*, 34654−34659.
31. Lad, L., Wang, J., Li, H., Friedman, J., Bhaskar, B., Ortiz de Montellano, P. R., and Poulos, T. L. (2003) Crystal structures of the ferric, ferrous, and ferrous-NO forms of the Asp140Ala mutant of human heme oxygenase-1: catalytic implications, *J. Mol. Biol. 330*, 527−538.
32. Zhou, H., Migita, C. T., Sato, M., Sun, D. Y., Zhang, X. H., Ikeda-Saito, M., Fujii, H., and Yoshida, T. (2000) Participation of carboxylate amino acid side chain in regiospecific oxidation of heme by heme oxygenase, *J. Am. Chem. Soc. 122*, 8311−8312.

33. Liu, Y., Lightning, L. K., Huang, H. W., Moenne-Loccoz, P., Schuller, D. J., Poulos, T. L., Loehr, T. M., and Ortiz de Montellano, P. R. (2000) Replacement of the distal glycine 139 transforms human heme oxygenase-1 into a peroxidase, *J. Biol. Chem. 275*, 34501−34507.
34. Torpey, J., and Ortiz de Montellano, P. R. (1996) Oxidation of the *meso*-methylmesoheme regioisomers by heme oxygenase, *J. Biol. Chem. 271*, 26067−26073.
35. Schuller, D. J., Wilks, A., Ortiz de Montellano, P. R., and Poulos, T. L. (1998) Crystallization of recombinant human heme oxygenase-1, *Protein Sci. 7*, 1836−1838.
36. Leslie, A. W. G. (1992) Joint CCP + ESF-EAMCB, *Newsletter on Protein Crystallography*.
37. Otwinowski, Z., and Minor, W. (1997) Processing of X-ray diffraction data collected in oscillation mode, *Methods Enzymol. 276*, 307−326.
38. Vagin, A., and Teplyakov, A. (1997) MOLREP: an automated program for molecular replacement, *J. Appl. Crystallogr. 30*, 1022−1025.
39. Schuller, D. J., Wilks, A., Ortiz de Montellano, P. R., and Poulos, T. L. (1999) Crystal structure of human heme oxygenase-1, *Nat. Struct. Biol. 6*, 860−867.
40. Brunger, A. T., Adams, P. D., Clore, G. M., DeLano, W. L., Gros, P., Grosse-Kunstleve, R. W., Jiang, J.-S., Kuszewski, R. F., Nilges, M., Pannu, N. S., Read, R. J., Rice, R. J., Rice, L. M., Simonson, T., and Warren, G. L. (1998) Crystallography & NMR System: A new software suite for macromolecular structure determination, *Acta Crystallogr. D54*, 905−921.
41. Jones, T. A., Zou, J. Y., Cowan, S. W., and Kieldgaard, M. (1991) Improved methods for binding protein models in electron density maps and the location of errors in these models, *Acta Crystallogr. D54*, 1017−1019.
42. Laskowski, R. A., MacArthur, M. W., Moss, D. S., and Thornton, J. M. (1993) PROCHECK: a program to check the stereochemical quality of protein structures, *J. Appl. Crystalogr. 26*, 283−291.
43. Lightning, L. K., Huang, H.-w., Moënne-Loccoz, P., Loehr, T. M., Schuller, D. J., Poulos, T. L., and Ortiz de Montellano, P. R. (2001) Disruption of an active site hydrogen bond converts human heme oxygenase-1 into a peroxidase, *J. Biol. Chem. 276*, 10612−10619.
44. Wagner, U. G., Muller, N., Schmitzberger, W., Falk, H., and Kratky, C. (1995) Structure determination of the biliverdin apomyoglobin complex: crystal structure analysis of two crystal forms at 1.4 and 1.5 Å resolution, *J. Mol. Biol. 247*, 326−337.
45. Pereira, P. J., Macedo-Ribeiro, S., Parraga, A., Perez-Luque, R., Cunningham, O., Darcy, K., Mantle, T. J., and Coll, M. (2001) Structure of human biliverdin IXb reductase, an early fetal bilirubin IXb producing enzyme, *Nat. Struct. Biol. 8*, 215−220.
46. Sheldrick, W. S. (1976) Crystal and molecular structure of biliverdin dimethyl ester, *J. Chem. Soc., Perkin Trans. 2*, 1457−1462.
47. Zhang, X., Fujii, H., Matera, M., Migita, C. T., Sun, D., Sato, M., Ikeda-Saito, M., and Yoshida, T. (2003) Steroselectivity of each of the three steps of the heme oxygenase reaction: hemin to *meso*-hydroxyhemin, *meso*-hydroxyhemin to verdoheme, and verdoheme to biliverdin, *Biochemistry 42*, 7418−7426.
48. Liu, Y., and Ortiz de Montellano, P. R. (2000) Reaction intermediates and single turnover rate constants for the oxidation of heme by human heme oxygenase-1, *J. Biol. Chem. 275*, 5297−5307.
49. Wang, J., and Ortiz de Montellano, P. R. (2003) The binding sites of human heme oxygenase-1 for cytochrome P450 reductase and biliverdin reductase, *J. Biol. Chem 278*, 20069−20076.
50. Kraulis, P. J. (1991) MOLSCRIPT: a program to produce both detailed and schematic plots of protein structure, *J. Appl. Crystallogr. 24*, 946−950.
51. Merritt, E. A., and Bacon, D. J. (1997) Raster3D−photorealistic molecular graphics, *Methods Enzymol. 277*, 505−524.

BI035451L